2021 43rd Annual International Conference of the
IEEE Engineering in Medicine & Biology Society (EMBC)
Oct 31 - Nov 4, 2021. Virtual Conference

Analysis of tumour microstructure estimation from conventional diffusion MRI and application to skull-base chordoma*

Morelli L., Buizza G., Palombo M., Riva G., Fontana G., Imparato S., Iannalfi A., Orlandi E., Paganelli C., Baroni G.

Abstract — **Skull-base chordoma (SBC) is a rare tumour whose molecular and radiological characteristics are still being investigated. In neuro-oncology microstructural imaging techniques, like diffusion-weighted MRI (DW-MRI), have been widely investigated, with the apparent diffusion coefficient (ADC) being one of the most used DW-MRI parameters due to its ease of acquisition and computation. ADC is a potential biomarker without a clear link to microstructure. The aim of this work was to derive microstructural information from conventional ADC, showing its potential for the characterisation of skull-base chordomas. Sixteen patients affected by SBC, who underwent conventional DW-MRI were retrospectively selected. From mono-exponential fits of DW-MRI, ADC maps were estimated using different sets of b-values. DW-MRI signals were simulated from synthetic substrates , which mimic the cellular packing of a tumour tissue with well-defined microstructural features. Starting from a published method, an error-driven procedure was evaluated to improve the estimates of microstructural parameters obtained through the simulated signals. A quantitative description of the tumour microstructure was then obtained from the DW-MRI images. This allowed successfully differentiating patients according to histologically-verified cell proliferation information.**

Clinical Relevance — **The impact on cancer management derives from the expected improvement of radiation treatment quality tailored to a patient-specific non-invasive description of tumour microstructure.**

I. INTRODUCTION

The treatment of rare, slow-growing and aggressive tumours, like skull-base chordoma (SBC), benefits from particle therapy which exploits carbon ions or protons instead of X-rays, as in conventional radiotherapy [1]. However, a full molecular and radiological characterisation of SBC is not yet available, preventing an optimal treatment definition. For these reasons, a deeper understanding of microstructural features would positively contribute to the current SBC characterisation, enabling treatment personalisation [2–9].

Diffusion-weighted magnetic resonance imaging (DW-MRI) is showing promising perspectives in radiotherapy applications, spanning from tumour characterisation to treatment personalisation [2–10]. DW-MRI is indeed suitable for indirectly characterising tissues at a microscopic scale (microstructure) through biophysical models or signal representations. Among these, we find simple mono-exponential models (e.g. conventional DW-MRI described by the ADC, Apparent Diffusion Coefficient, or diffusion tensor imaging, DTI), as well as more complex models such as multi-compartmental [11–13], and others [14], that provide information on diffusivity, vascularity, density, or cell size. The richer description, however, requires challenging and longer acquisition protocols, which are often not feasible within radiotherapy imaging, that mostly encodes coarser and non-specific microstructural information through conventional ADC. Recently, a computational approach [15] has been proposed to overcome the limitations of simplistic DW-MRI acquisitions, conventionally employed in radiotherapy imaging. Using Monte Carlo simulations of particles diffusion in virtual tumour-like environments, the approach estimates indices of microstructural features such as cell size and density, and water apparent diffusivity from conventional ADC data.

The aim of this study was, therefore, to evaluate the framework to derive improved microstructural information from conventional DW-MRI [15] and characterise SBC treated with particle therapy.

II. METHODS

A. DW-MRI acquisition

Sixteen patients affected by SBC, who underwent DW-MRI (b-values=50,400,1000 smm^{-2}, averaged 3 orthogonal directions, Magnetom Verio – Siemens, Erlangen) before treatment and who were enrolled for particle therapy at the National Center of Oncological Hadrontherapy (CNAO), were retrospectively selected. The study was approved by the local Research Ethics Board. From mono-exponential fits of DW-MRI, ADC maps were estimated using b=50,1000, b=400,1000 and b=50,400,1000 smm^{-2}. Gross target volume (GTV) contours and histological information (proliferation index Ki-67) were collected.

B. Numerical DW-MRI simulations

Following the approach described in [15], DW-MRI signals (N=3928) were simulated using Monte Carlo simulations [16], and the same acquisition parameters used in the SBC cohort, with ADCs computed using b=50,1000, b=400,1000 and b=50,400,1000 smm^{-2}. Signals were

*Research supported by AIRC (Associazione Italiana per la Ricerca sul Cancro), Investigator Grant-IG 2020, project number 24946.

LM is with Department of Electronics, Information and Bioengineering (DEIB), Politecnico di Milano, Milan, Italy (corresponding author to provide phone: +390223999022; e-mail: letizia.morelli@mail.polimi.it).

GBu, CP and GBa are with Department of Electronics, Information and Bioengineering (DEIB), Politecnico di Milano, Milan, Italy.

MP is with Centre for Medical Image Computing (CMIC), Department of Computer Science, University College London (UCL), London.

GR, GF, SI, AI, EO and GBa are with National Center of Oncological Hadrontherapy (CNAO), Pavia, Italy.

simulated from synthetic substrates that mimic the cellular packing of tumour tissues as aggregated ellipsoids with well-defined density and geometrical properties (range: cells' radius (R) 2.5-10.0 μm; volume fraction (vf) 0.3-0.6; diffusivity (D) 0.5-3.0 μm^2/ms).

C. From ADC to microstructure

As in [15], after partitioning the simulated ADCs, input data were modelled as a weighted sum of the partitions' centroid, where each weight W quantifies the contribution of a cluster to the overall estimate. These weights were determined through an optimisation procedure and then used to estimate the microstructural parameters (R, vf, D) of the input data.

D. Improving the estimates of microstructural parameters

An error-driven procedure was evaluated to improve the estimates of microstructural parameters. The absolute estimation error of the microstructural parameters (difference between true and estimated value) was computed for the simulated data, whose true values were known. In particular, the procedure involved: (i) calculating the absolute estimation errors, comparing true values and initial parameters estimates, for the simulated data; (ii) initially estimating microstructural parameters for input data; (iii) considering a set of n first-neighbour simulations close (in terms of ADCs and set of weights: dist(ADC,W)) to the input data to calculate the mean value of the absolute errors; (iv) adding this average error to the initial estimates.

E. Accuracy analyses and application to SBC patients' data

The accuracy of the method, with or without error correction, was assessed in terms of root mean square error (RMSE) on a random sample of the simulations (training-set 80%, test-set 20%). Then, the ranges of the estimated microstructural parameters in the two cases were compared with that of the true values, known by design.

Accuracy was also exploited for sensitivity analyses, aiming at defining the optimal free parameters of the correction procedure, i.e., the number n of closest simulations, the dimension of the training set and the type of distance to be used to calculate the corrective error. The standard deviation (SD) of the parameters from n close simulations was computed to evaluate the behaviour of the introduced local error correction procedure.

Finally, the model was applied voxel-wise to patients' GTVs to produce quantitative maps of R, vf and D. Histogram-based metrics (mean, median, interquartile range, entropy) were compared between patients with high (Ki-67≥5%) or low (Ki-67<5%) proliferation through statistical tests (Mann-Whitney U-test, α=0.05).

III. RESULTS

The RMSE calculated on the test-set, separately for each parameter, showed that accuracy improves after the correction procedure (Fig. 1). The improvement in performance was also confirmed by the estimated parameters' ranges, that better followed the ranges of true values after the error correction procedure (Fig. 2), with stark improvements for R and vf.

Sensitivity analyses for the definition of free parameters showed that the best result, across all microstructural parameters, was obtained with n=4 close simulations (Fig. 3) and a distance that considered both ADCs and the set of weights (Fig. 4).

The parameters' SD of the n=4 simulations used for the correction reached high values (up to 3.44 μm, 0.15 and 0.54 μm^2/ms, for R, vf and D, respectively),

From the voxel-wise maps obtained by applying the model (Fig. 5) to the patients' GTV and from the analysis of the histogram metrics, significant statistical differences were found for entropy values (statistically significant for R (p=0.021), vf (p=0.021) and D (p=0.035), but not for the measured ADC (p=0.106)), with GTVs characterised by high cell proliferation being described by high entropy (Fig. 6).

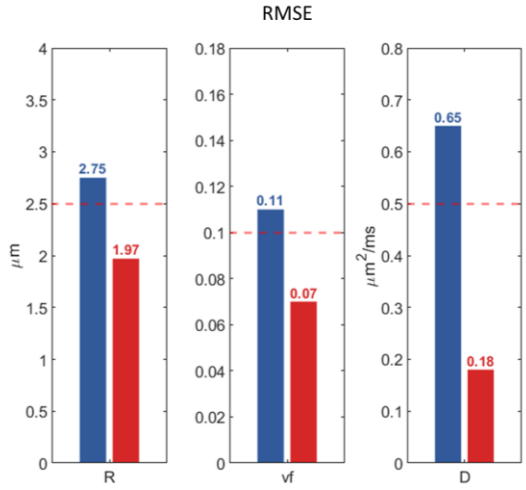

Figure 1. Comparison of RMSE obtained for simulations before (blue) and after (red) the correction procedure employing the absolute estimation error. The dashed red lines indicate the resolution at which parameters were defined (2.5 μm for R, 0.1 for vf and 0.5 for D).

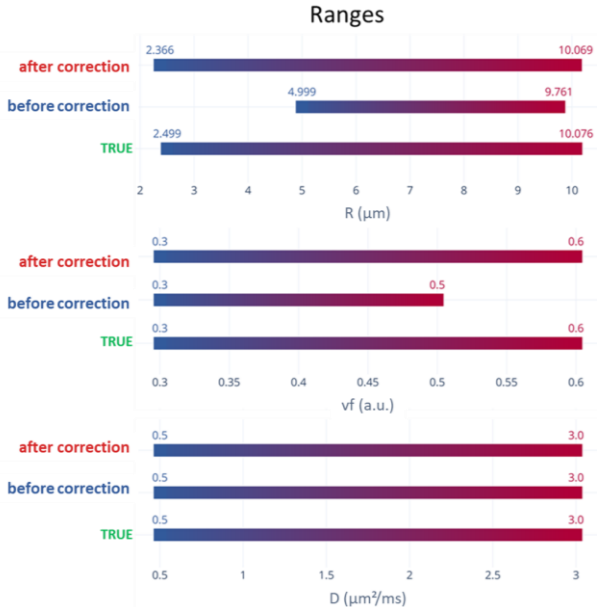

Figure 2. Ranges of microstructural parameters estimates for R, vf and D. For each parameter, the range of true values (bottom row), estimated values before (middle row) and after error correction (top row) are shown.

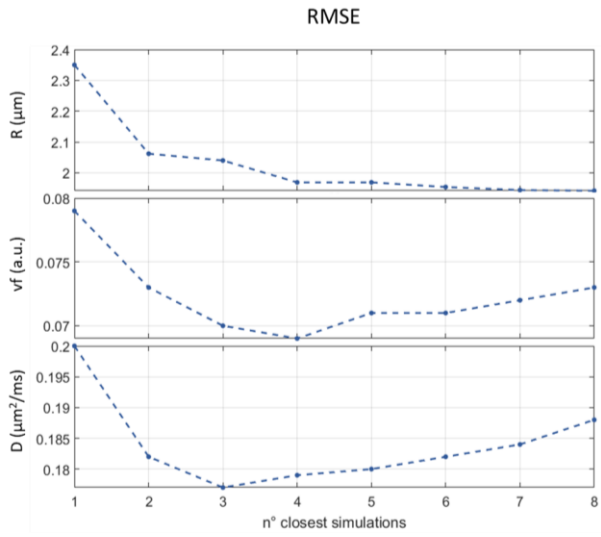

Figure 3. RMSE performance as the number of closest simulations (n) used to correct the parameters' estimate increases from 1 to 8.

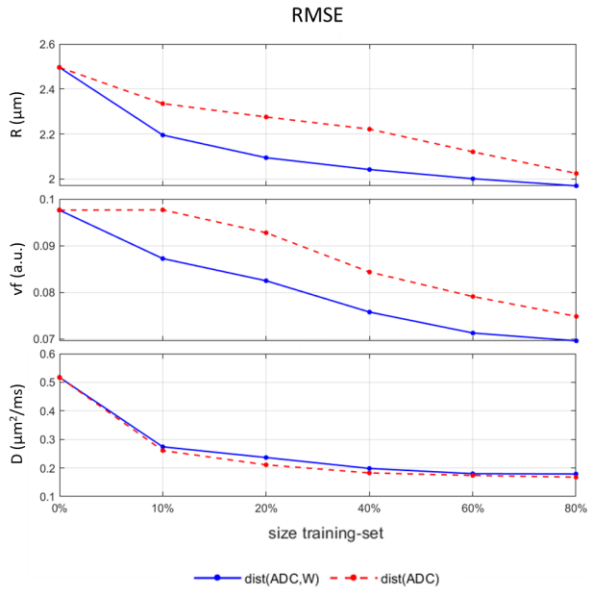

Figure 4. RMSE for R, vf and D as a function of the size of the training set (expressed in terms of % of the total available simulations) used for estimating the corrective error, comparing the case when the correction uses a distance that depends on ADC and the set of weights (dist(ADC,W), solid blue) or only on ADC coordinates (dist(ADC), dashed red). The values at 0% refer to the RMSE obtained without correction.

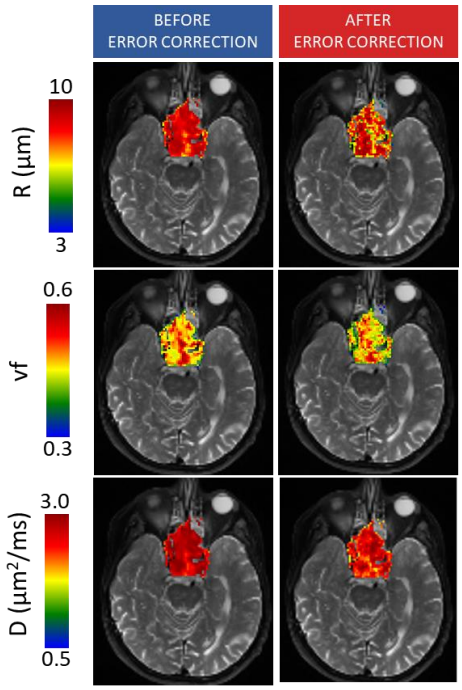

Figure 5. ADC-derived microstructural maps in an example patient before (left) and after (right) estimation error correction. After correction, a higher spatial heterogeneity is visible.

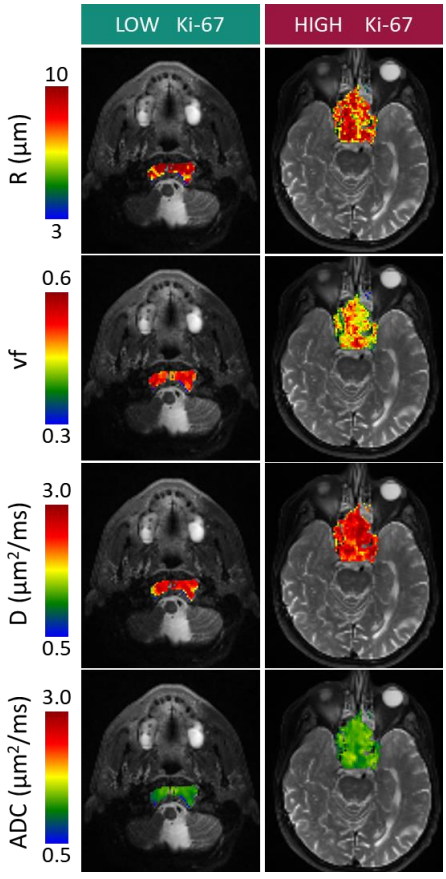

Figure 6. Examples of microstructural maps from two patients characterised by low (Ki-67<5%, left) or high (Ki-67≥ 5%, right) cell proliferation indices.

IV. DISCUSSION AND CONCLUSION

In this work, microstructural features were inferred from ADC data, using a previously published computational approach [15] to characterise the ADC-microstructure relationship in terms of predefined tissue features (R, vf, D).
In this work, a new procedure to reduce the estimation error was proposed within the framework from [15] and a quantitative description of the tumour microstructure in terms of R, vf and D, was obtained from conventional DWI widely available in clinical settings, instead of complex models (e.g. VERDICT [13]) which require richer MRI acquisitions often not compatible with standard clinical protocols.
By applying the proposed correction to simulation data, the RMSE on the estimates dropped below the resolution at which parameters were defined (2.5 μm for R, 0.1 for vf and 0.5 for D), whereas errors from the original method in [15] yielded higher values. Such correction also allowed restoring the full range of the microstructural parameters. The importance of the training dataset was highlighted by the sensitivity analyses conducted for dist(ADC,W), that showed decreasing errors when increasing the size of the training-set [17]. Also, the estimation error decreased when considering n=4 closest simulations. The high values of the parameters' SD of the n=4 simulations confirmed the non-specific association of the ADC to the underlying microstructure, for which similar ADCs can point to very different microstructure configurations. This also suggested that the proposed correction procedure did not introduce a systematic bias: the n=4 simulations involved in the correction did not force the estimate on which they acted to assume a consistently different value but, rather, they corrected the estimate by compensating it with the average error that the model commits in that region.

Although further validation (in histopathological, clinical, and technical terms) of the method is needed, this work quantified the error associated to the estimation of microstructural parameters derived by the simulation framework in [15] and proposed a novel procedure with which the estimation error can be reduced.

The potential clinical value of the method was shown in the context of SBC, as patients with high or low cell proliferation were successfully discriminated using R, vf and D, in contrast to conventional ADC. The quantitative maps of microstructural parameters derived after error correction showed also higher spatial variability with respect to ADC, pointing towards a potentially improved detection of microstructure heterogeneity. Future studies will be performed on a wider patient cohort, to validate the current findings.

In conclusion, the adopted framework allowed deriving accurate microstructural parameters and can be easily translated on conventional ADC data widely available in clinical radiotherapy settings. Furthermore, the application on SBC tumour showed its potential to non-invasively characterize the proliferative capacity in SBC and contribute to treatment personalisation in particle therapy.

ACKNOWLEDGMENT

The authors would like to thank Associazione Italiana per la Ricerca sul Cancro (AIRC IG 2020 – 24946) for the support. The authors also thank Luca Anemoni for his valuable support in data collection and curation. Marco Palombo is supported by UKRI Future Leaders Fellowship (MR/T020296/1).

REFERENCES

[1] A. Iannalfi *et al.*, "Proton and carbon ion radiotherapy in skull base chordomas: a prospective study based on a dual particle and a patient-customized treatment strategy," *Neuro. Oncol.*, vol. 22, no. 9, pp. 1348–1358, 2020, doi: 10.1093/neuonc/noaa067.

[2] S. Leibfarth *et al.*, "Potentials and challenges of diffusion-weighted magnetic resonance imaging in radiotherapy," *Clinical and Translational Radiation Oncology*, vol. 13. Elsevier Ireland Ltd, pp. 29–37, Nov. 01, 2018, doi: 10.1016/j.ctro.2018.09.002.

[3] D. T. Ginat *et al.*, "Diffusion-Weighted Imaging for Differentiating Benign From Malignant Skull Lesions and Correlation With Cell Density," *Am. J. Roentgenol.*, vol. 198, no. 6, pp. W597–W601, Jun. 2012, doi: 10.2214/AJR.11.7424.

[4] D. M. Patterson *et al.*, "Technology Insight: Water diffusion MRI - A potential new biomarker of response to cancer therapy," *Nature Clinical Practice Oncology*, vol. 5, no. 4. Nature Publishing Group, pp. 220–233, Apr. 26, 2008, doi: 10.1038/ncponc1073.

[5] D. P. Noij *et al.*, "Predictive value of diffusion-weighted imaging without and with including contrast-enhanced magnetic resonance imaging in image analysis of head and neck squamous cell carcinoma," *Eur. J. Radiol.*, vol. 84, no. 1, pp. 108–116, Jan. 2015, doi: 10.1016/j.ejrad.2014.10.015.

[6] H. Bae *et al.*, "Apparent diffusion coefficient value as a biomarker reflecting morphological and biological features of prostate cancer," *Int. Urol. Nephrol.*, vol. 46, no. 3, pp. 555–561, Sep. 2014, doi: 10.1007/s11255-013-0557-1.

[7] S. Kim *et al.*, "Diffusion-weighted magnetic resonance imaging for predicting and detecting early response to chemoradiation therapy of squamous cell carcinomas of the head and neck," *Clin. Cancer Res.*, vol. 15, no. 3, pp. 986–994, Feb. 2009, doi: 10.1158/1078-0432.CCR-08-1287.

[8] S. Marzi *et al.*, "Early radiation-induced changes evaluated by intravoxel incoherent motion in the major salivary glands," *J. Magn. Reson. Imaging*, vol. 41, no. 4, pp. 974–982, Apr. 2015, doi: 10.1002/jmri.24626.

[9] H. C. Thoeny and B. D. Ross, "Predicting and Monitoring Cancer Treatment Response with Diffusion-Weighted MRI," *J. Magn. Reson. Imaging*, vol. 16, pp. 2–16, 2010, doi: 10.1002/jmri.22167.

[10] O. J. Gurney-Champion *et al.*, "Quantitative imaging for radiotherapy purposes," *Radiother. Oncol.*, vol. 146, pp. 66–75, 2020, doi: 10.1016/j.radonc.2020.01.026.

[11] D. S. Novikov *et al.*, "On modeling," *Magn. Reson. Med.*, vol. 79, no. 6, pp. 3172–3193, Jun. 2018, doi: 10.1002/mrm.27101.

[12] L. Tang and X. J. Zhou, "Diffusion MRI of cancer: From low to high b-values," *J. Magn. Reson. Imaging*, vol. 49, no. 1, pp. 23–40, 2019, doi: 10.1002/jmri.26293.

[13] E. Panagiotaki *et al.*, "Noninvasive Quantification of Solid Tumor Microstructure Using VERDICT MRI," *Cancer Res.*, vol. 74, no. 7, pp. 1902–1912, Apr. 2014, doi: 10.1158/0008-5472.CAN-13-2511.

[14] O. Reynaud, "Time-Dependent Diffusion MRI in Cancer : Tissue Modeling and Applications," *Front. Phys.*, vol. 5, no. November, pp. 1–16, Nov. 2017, doi: 10.3389/fphy.2017.00058.

[15] G. Buizza *et al.*, "Improving the characterization of meningioma microstructure in proton therapy from conventional apparent diffusion coefficient measurements using Monte Carlo simulations of diffusion MRI," *Med. Phys.*, vol. 48, no. 3, 2021, doi: 10.1002/MP.14689.

[16] P. A. Cook *et al.*, "Camino: Open-Source Diffusion-MRI Reconstruction and Processing," *14th Sci. Meet. Int. Soc. Magn. Reson. Med.*, vol. 14, p. 2759, 2006.

[17] N. G. Gyori *et al.*, "Training Data Distribution Significantly Impacts the Estimation of Tissue Microstructure with Machine Learning," *bioRxiv*, p. 2021.04.13.439659, Apr. 2021, doi: 10.1101/2021.04.13.439659.